Effects of nanostructure geometry on polymer chain alignment and device performance in nanoimprinted polymer solar cell

Yi Yang[a], Kamil Mielczarek[b], Anvar Zakhidov[a,b], Walter Hu*[a,c]

[a]Department of Materials Science and Engineering; [b]Department of Physics; [c]Department of Electrical Engineering, The University of Texas at Dallas, 800 W. Campbell Road, Richardson, TX USA 75080-3021

ABSTRACT

Among the various organic photovoltaic devices, the conjugated polymer/fullerene approach has drawn the most research interest. The performance of these types of solar cells is greatly determined by the nanoscale morphology of the two components (donor/acceptor) and the molecular orientation/crystallinity in the photoactive layer. This article demonstrates our recent studies on the nanostructure geometry effects on the nanoimprint induced poly(3-hexylthiophene-2,5-diyl) (P3HT) chain alignment and photovoltaic performance. Out-of-plane and in-plane grazing incident X-ray diffractions are employed to characterize the chain orientations in P3HT nanogratings with different *widths* and *heights*. It is found that nanoimprint procedure changes the initial edge-on alignment in non-imprinted P3HT thin film to a vertical orientation which favors the hole transport, with an organization *height* $H \gtrsim$ 170 nm and *width* in the range of 60 nm$\leq$ $W<$ 210 nm. Samples with better aligned molecules lead to a larger crystallite sizes as well. Imprinted P3HT/[6,6]-penyl-C61-butyric-acid-methyl-ester (PCBM) solar cells show an increase in power conversion efficiency (PCE) with the decrease of nanostructure *width*, and with the increase of *height* and junction area. Devices with the highest PCE are made by the fully aligned and highest P3HT nanostructures (*width* $w=$ 60 nm, *height* $h=$ 170 nm), allowing for the most efficient charge separation, transport and light absorption. We believe this work will contribute to the optimal geometry design of nanoimprinted polymer solar cells.

Keywords: polymer solar cell, chain alignment, nanoscale morphology, nanoimprint lithography, nanostructure geometry

1. INTRODUCTION

Conjugated polymers based organic photovoltaics (OPVs) have been subject to increasing research interest over the past years due to the potential of being light weight, mechanically flexible, semitransparent as well as the relatively high power conversion efficiency (PCE) when compared to other types of OPVs such as small molecule solar cells.[1-2] However, the highest PCE achieved by this type of solar cells is still lower than their inorganic counterparts.[3] The first challenge for higher efficiency arises from the difficulty to achieve a precisely controlled donor/acceptor phase separation within the short exciton diffusion length (~10 nm) without dead ends.[4-5] So far it has been impossible to achieve such a morphology in the most widely used bulk heterojunction (BHJ) structure in which randomly distributed phases cause significant charge recombination.[6] A second reason for the inferior performance of polymer solar cells is the low charge mobility, especially the hole mobility ($\mu_h \sim 10^{-6-10-3}$ cm^2/V·s) within the donor polymer, as compared to the inorganic photovoltaic materials.[7-8] In recent years, nanoimprint lithography (NIL) has been regarded as an effective technique to simultaneously solve these issues.[9-12] For example, with this technique, the ideal morphology, *i.e.,* ordered and interdigitized heterojunction, can be realized between poly(3-hexylthiophene-2,5-diyl) (P3HT) and [6,6]-penyl-C61-butyric-acid-methyl-ester (PCBM), the most commonly studied donor-acceptor combination.[13-16] Moreover, a NIL induced molecule organization for P3HT has been observed by different groups, indicating its potential to improve hole mobility in aligned polymer chains.[17-19] Better PCEs over non-imprinted bilayer devices have been reported using this novel approach and thus demonstrated its great potential for highly efficient devices.

However, it is noted that various geometries of imprinted P3HT nanostructures have been used in different groups, leading to different sizes/shapes of donor/acceptor junctions and thus solar cell efficiencies.[9] It is therefore difficult to compare the results of one work to another and understand the nanostructure geometry effects. Moreover, people haveconfirmed that during the imprint of polymers like polyvinylidene fluoride (PVDF) and poly(9,9-dioctylfluorene-co-benzothiadiazole) (F8BT), crystallization happens starting from the regions close to the mold trench walls and there are maximum sizes for this chain reordering regions.[20-21] Therefore it is important to confirm if there is also a size limit for P3HT chain alignment beyond which only partial alignment occurs. In our previous work, we speculated that the chain alignment width would be approximately 100 nm according to the effect of surfactant on P3HT chain orientations and charge mobility.[17, 22]

In this work, to confirm these speculations, we first systemically studied the nanostructure geometry effect on chain orientation by the grazing incident X-ray diffraction (GIXRD) measurements of P3HT nanogratings with different *widths* and *heights*. It was found that a vertical orientation favoring the hole transport was formed in imprinted P3HT nanogratings with an organization *height H*≥ 170 nm and *width* in the range of 60 nm≤ *W* < 210 nm. Then P3HT/PCBM solar cells with different *widths* and *heights* of P3HT nanograting were fabricated to study their influences on device performance. The highest PCE was observed on devices with the fully aligned and highest nanostructures (*w*= 60 nm, *h*= 170 nm), which was enable by the most efficient charge separation, transport and light absorption.

2. EXPETRIMENTAL SECTION

2.1 GIXRD measurement of P3HT nanogratings

P3HT (Reike Metal, Ltd.) thin films were spincoated on P-type (100) Si substrates and imprinted at 170 °C and 50 MPa for 600 sec. As summarized in Table 1, six different geometries of P3HT structures were made in this work to study the *width* and *height* effects on chain alignment and solar cell performance. It should be noted that G1, 70 nm non-imprinted thin film, was used as reference and the same thickness as G2, G3 and G5 before they were imprinted into nanostructures. The same thickness of *residual layer* (*f*= 20 nm) was intentionally made for all geometries to equalize its effects. The initial thickness, L_0, to fabricate nanogratings with *height h*, *width w*, *spacing p* and *residual layer f* can be approximately calculated by

$$L_0 = \frac{wh}{w+p} + f \quad , \tag{1}$$

It is noted that there is a constant increase in the interface enhancement factor (IEF), which describes the ratio of imprinted nanostructure interface area (A) to non-imprinted one (A_0),

$$IEF = A/A_0 = 1 + \frac{2h}{w+p} \quad , \tag{2}$$

from G1 to G6[12].

GIXRD measurement was carried out to measure the P3HT chain alignments using a Rigaku Ultima III diffractometer with a wavelength of 0.154 nm. To find the geometry effects of P3HT nanostructures on each organization direction by NIL, two types of GIXRD setups, *i.e.,* out-of-plane and in-plane, were employed to provide a three-dimensional view of chain orientation within imprinted nanogratings.[17, 23] As shown in Figure 1(a), in out-of-plane GIXRD, the detector is rotated vertically with respect to the sample surface with a scan axis of *2θ*, so that only the chain alignment along the *z* direction can be studied. While for in-plane measurement, as shown in Figure 1(b), both sample stage and detector are rotated horizontally with scan axes of *ϕ* and *2θχ*, respectively, so that the crystallite information along the *x* and *y* directions can be obtained. In in-plane measurement, the nanograting direction was adjusted parallelly or perpendicularly to the incident X-ray beam manually with the cross hair labelled on the sample stage. In both out-of-plane and in-plane measurements, the angular spectrum was collected from 3° to 30°. A small incident angle (*ω*= 0.5°) which was slightly larger than the critical angle of P3HT (*a_c*= 0.16°) to the sample surfaces was used to make sure the beam can penetrate samples with different thicknesses, without hitting the substrate underneath.[24-25]

2.2 Solar cell fabrication and characterization

P3HT/PCBM solar cells with different feature sizes of P3HT nanogratings as listed in Table 1 were fabricated in the following structure: indium tin oxide ITO/poly(3,4-ethylenedioxythiophen): polystyrene sulfonic acid (PEDOT:PSS)/P3HT/PCBM/LiF/Al. First a thin layer (~20 nm) of PEDOT:PSS (CLEVIOS P VP Al 4083, H. C. Starck, Inc.) was spin-coated onto patterned ITO coated glass substrates (Luminescence Technology) and baked at 150 °C for 15 min. In this work, low conductive PEDOT:PSS was chosen to minimize the measurement error from device areas due to the lateral conductivity of PEDOT:PSS.[26] Then P3HT nanogratings with different geometries were formed on top by nanoimprint under the same condition as GIXRD measurement, followed by the spincoating of 120 nm PCBM (Nano-C) from dichloromethane (DCM) which serves as an orthogonal solvent. Finally, 1 nm LiF and 100 nm Al were thermally evaporated on top as the cathode. Four solar cell pixels were formed on each substrate with an active area each of 9 mm^2. After the OPV devices were made, their current density-voltage (*J-V*) characteristics were measured using Air Mass 1.5 global solar simulated light (AM. 1.5G) calibrated using an NREL traceable KG5 color filtered silicon photodiode (PV Measurements Inc.) to an intensity of 100 mW/cm^2.

3. RESULTS AND DISCUSSIONS

3.1 Effects on chain alignment

As shown in Figure 2, for organic solar cells with the active layer vertically sandwiched between anode and cathode, it is preferable for polymers to align with an orientation which allows for a smaller hopping distance along the vertical electric field direction and a larger hole mobility. Among the three possible orientations for P3HT, edge-on is the least favorable due to the large hopping distance *a* (~1.69 nm) along the hexyl side chain which results in a very low hole mobility (10^{-10} cm^2/V·s). A large vertical hole mobility (~0.1 cm^2/V·s) becomes possible if a face-on or vertical orientation can be realized, with the short hopping distances *b* (~0.38 nm) and *c* (~0.38 nm) along the π-π stacking and backbone directions, respectively.[17, 27-31] Annealing the device at temperatures higher than the T$_g$ of P3HT (~80 °C) has been shown to allow the polymer chains to reorder in a more thermodynamically favorable way and increase its crystallinity.[32-34] However it is evident that during annealing, P3HT thin films tend to be aligned parallel to the substrate, *i.e.*, in edge-on orientation, and thus limit the vertical conductivity.[22, 30-31, 35] Our previous studies have shown that a vertical orientation can be realized using nanoimprint and it is thus possible to enhance the hole mobility with this technique.[14, 17] However, the maximum *width* for this NIL induced chain alignment and its effect on OPV performance remained unknown.

To find the size of NIL induced P3HT crystallites on each direction, out-of-plane and in-plane GIXRD measurements were used in this work. In the out-of-plane GIXRD, nanogratings G1, G5 and a 20 nm thin film which was as thick as the *residual layer* of all imprinted nanogratings were analyzed first. Before measurement, G1 and the 20 nm thin film were pressed by a flat Si mold at the same temperature and pressure as G5, so that any effect from the temperature or pressure induced crystallization would be ruled out. As shown in Figure 3(a1), (100) peaks at 5.2°, corresponding to lattice parameter *a*, were observed for all three samples but with different intensities, indicating that there were different amounts of edge-on orientations. The (100) peak for imprinted nanogratings G5 is much lower than that for G1 although they had the same thickness before imprint, suggesting that there was a change in the initial edge-on orientation after nanoimprint. Since there was no (010) peak corresponding to lattice paramtere *b* detected at 23.4° it is speculated that the primary chain orientation was vertical, which is consistent with literature.[36] When compared to the 20 nm thin film, the intensity of the (100) peak for G5 is slightly higher, indicating that there is still edge-on orientation within the nanogratings above their *residual layer*.

There are two possible answers to explain this result. The first possibility is that the *width* of nanoimprint induced chain alignment for P3HT is less than 60 nm, resulting in the molecules to be partially aligned, *i.e.*, edge-on, in the middle of the nanostructures. The second possibility is that the P3HT molecules are fully aligned within 60 nm nanostructures. However, since the alignment remains edge-on within the *residual layer* (results not shown but confirmed in our work) while it is vertical inside the nanogratings above, there might be a transition region (most likely within the lower part of the nanostructures) where both edge-on and vertical orientations exist, leading to a higher (100) peak for G5. To find out which possibility is

correct, an additional three geometries (G3, G4 and G6) were tested for comparison, as shown in Figure 3(a2). It can be seen that compared to the (100) peak in G5, those in G4 and G6 show almost the same intensities, indicating that the second possibility is the real reason: all three nanostructures G4 to G6 share the same *width/spacing* and *residual layer*, which results in the same amount of edge-on orientation within the transition region and *residual layer*. This result also suggests that there must be a full chain alignment within 60 nm wide P3HT nanostructures. The first possibility cannot be true, otherwise the shorter G4 and taller G6 samples should have lower and higher (100) peak intensities respectively due to the fact that crystallization by NIL starts from the regions close to the mold trenches.[21] It can also be seen that G3, which has the same nanograting *height* but a much larger *width*, shows a larger (100) peak than G5. This is because the chain alignment *width* is less than 210 nm and P3HT molecules were not fully aligned within such wide nanostructure. Therefore we can conclude that the range of P3HT chain alignment *width* by NIL is equal or larger than 60 nm but smaller than 210 nm, consistent to the range which people have found for surfactant induced P3HT chain alignment in transistors.[22]

To confirm the vertical chain alignment by nanoimprint and the range of organization *width* in-plane GIXRD measurements were also performed on G3 to G6 with gratings parallel and perpendicular to the incident beam, as shown in Figure 3(b1) and 3(b2), respectively. When the analysis is done in parallel, all nanostructures show large (100) peaks and ultra-low (010) peaks. However, when measured in the perpendicular orientation, all (100) peaks are quenched and larger (010) peaks present. These results demonstrate that P3HT chains after nanoimprint were vertically aligned, with hexyl side chain *spacing a* perpendicular to and π-π stacking *b* along the grating direction. The tiny (010) peaks in Figure 3(b1) and (100) peaks in Figure 3(b2) are believed to be from the finite alignment variations, which have been observed in literature.[17] It is worth noting that in both figures one can observe the amount of variation in G6 is the same as in G4 and G5 even though the nanostructures in G6 are the highest. This suggests that the arrangement of P3HT chains became more regular with respect to the gratings as the polymer flowed higher into the mold cavities. It can also be seen that there is a constant increase in both (100) and (010) peak intensities in Figure 3(b1) and 3(b2), with the nanograting *height* from G4 to G6, demonstrating that the chain alignment *height H* by NIL can be up to 170 nm. Compared to all other samples, G3 shows the lowest peaks intensity in both in-plane measurements. A possible explanation could be that the edge-on alignment within the partially aligned G3 is only ordered with lattice parameter *a* along the z axis, but disordered along the x and y axes, which has been proven in literature.[17] It thus gives G3 the highest peak in the out-of-plane measurement, but the lowest in the in-plane measurements (lowest density of vertical alignment).

Therefore, the in-plane XRD results confirm our conclusions made from the out-of-plane measurement, *i.e.*, nanoimprint can change the initial edge-on alignment in non-patterned thin film to vertical, with an organization *width* of 60 nm≤ *W*< 210 nm and *height H*≥ 170 nm. A schematic overview of partially and fully aligned P3HT molecules within different sizes of nanostructures is provided in Figure 4. It can be seen that high and narrow P3HT nanostructures like G6 are the optimal for OPVs because of the largest density of vertical orientations and thus possibly highest vertical hole mobility.

In XRD spectra above, the *height* of each peak is proportional to the total number of P3HT crystallites per unit volume, *i.e.*, the crystallinity in the specific direction. The size of NIL formed P3HT crystallites *L* can be obtained by the Scherrer formula

$$L \sim \frac{0.9\lambda}{\Delta_{2\theta}\cos(\theta)} \ , \tag{3}$$

where λ is the X-ray wavelength and $\Delta_{2\theta}$ is the full *width* half maximum of the peak.[29-30, 37] Applying equation (2) to (100) peaks in Figure 3(b1) and (010) peaks in Figure 3(b2) which illustrate the main chain alignment by NIL, one can obtain the crystallite sizes L_a and L_b for G3 to G6 along directions *a* and *b*, respectively. As summarized in Table 2, the crystallite size increases with nanostructure *height* but decreases with nanostructure *width* in both *a* and *b* directions, suggesting that a higher density of vertical alignment leads to a larger size of crystallite as well. It also indicates that the hole mobility in D6 would be the highest and thus this geometry would be the best for solar cells.

3.2 Effects on solar cell performance

To study the nanostructure geometry effect on OPV performance and further confirm that a structure in G6 would be the optimal among all studied geometries, P3HT/PCBM solar cells with different feature sizes of P3HT nanogratings as listed in Table1 were made. The *J-V* characteristics of these devices are shown in Figure 5. Open circuit voltage (V_{oc}), short circuit current (J_{sc}), fill factor (FF) and PCE of these devices were extracted from the *J-V* curves and listed in Table 3. For each device the results were calculated from the average of four OPV pixel devices on the same substrate and their standard deviations were calculated.

As shown in Figure 5, it is found that from D1 to D3 and D5 which have the same *height*, the J_{sc} increases constantly with the decrease of nanograting *width/spacing*. The first reason for this is due to the decreasing size of the nanostructures, *i.e.*, closer to the exciton diffusion length, resulting in better charge separation. The second reason for this improvement in photocurrent may come from the higher density of vertically aligned crystallites which leads to increased hole mobility within the narrower gratings, which has been shown in the previous GIXRD study. Enhanced hole mobility can also result in an increase in FF, which is dependent on the carrier drift length L_d,

$$L_d = \mu \tau E, \tag{4}$$

where μ is the carrier mobility, τ is the carrier lifetime and E is the electric field.[38] Hence a better FF can be expected if there is an increase in mobility within the same active layer thickness, which was observed for these devices, as shown in Figure 5. For D4 to D6 with the same *width/spacing*, they demonstrate similar FFs which might be attributed to fully aligned P3HT molecules within them. It is interesting that the FF in D6 shows the highest average value among all devices even though it has the largest *height* (170 nm). This means that the hole mobility or hole drift length in this device must be the highest so that the recombination losses are minimized. In Table 3 the device D6 shows the largest crystallite sizes which can be an explanation for the large FF values measured. It is also worth noting that FFs more than 60%, which are similar to the values in the BHJ structure are found in D6. A high FF in a BHJ device is possible because the hole and electron mobilities are more balanced due to the interaction between polymers and fullerenes.[32, 39] In bilayer solar cells in which the properties of polymers and fullerenes are more independent, μ_h is typically two to three orders of magnitude lower than electron mobility (μ_e), resulting in the hole accumulation at the anode and a space–charge limited current.[40] This photocurrent has a square-root dependence on bias, and thus a FF above 40% is difficult to achieve, as observed in D1.[41] The fabrication of nanoimprinted OPVs is similar to bilayer devices with fullerenes spincoated on top of the polymer, but still a high FF was achieved in D6, again indicating that there is a nanoimprint induced vertical mobility enhancement. Moreover, D6 shows the highest J_{sc} compared to D4 and D5, which might be due to the most efficient light absorption. The highest performance of D6 confirms our conclusion from GIXRD results that nanostructures with the smallest *width* but largest *height* are optimal for OPVs. Other than the impact of *width* and *height*, constant increases in J_{sc}, FF and PCE with IEF are also found which highlight the importance of a large donor-acceptor interfacial area, as shown in Figure 5. In this work the average PCE realized in D6 (~3.1%) is three times higher than the non-imprinted D1 (~1.16%) and similar to those typical values (~3-4%) reported in BHJ structure using the same materials. In this work, small standard deviations were demonstrated from each type of device as shown in Table 3. To further reduce the experimental errors, three batches of P3HT/PCBM solar cells with different sizes of P3HT nanogratings as listed in Table 1 were made. Similar correlations between geometry and device performance were observed for all devices.

A higher solar cell performance is believed to be achievable through further optimizations. Besides reducing the P3HT *residual layer* to minimize light screening and better collect holes, the PCBM thickness can also be optimized to better match hole transport. It is also highly likely to obtain a better PCE by further decreasing the P3HT nanostructure *width* (60 nm) to the exiton diffusion length by making sub 20 nm molds as well as increasing the *height*, as predicted by the trend found in this study. The geometry design for imprinted field effect transistors may also benefit from this work. It is worth noting that in this work, the effects of nanoimprint on mobility have been studied indirectly and based on the analysis of the results reported in literature and our speculations. To confirm our statements experimentally, the explicit vertical hole mobility in varied sizes of P3HT nanostructures are now being directly measured through conductive AFM and vertical transistors.

4. CONCLUSIONS

In summary, the effects of nanostructure geometry on nanoimprint induced P3HT chain alignment and photovoltaic performance were systemically studied. According to the out-of-plane and in-plane GIXRD measurements of P3HT nanogratings with different *widths* and *heights*, we found that the initial edge-on alignment in non-imprinted P3HT thin film was changed into a vertical orientation with an organization *height H≥* 170 nm and *width* in the range of 60 nm≤ *W<* 210 nm. Larger crystallite sizes were also found within samples with better aligned molecules. Imprinted P3HT/PCBM solar cells showed an increase in PCE with the decrease of nanostructure *width*, increase of *height* and IEF. Devices with the highest PCE were made using fully aligned and the highest P3HT nanostructures, which resulted in the most efficient charge transport and light absorption. A better design for nanoimprinted P3HT solar cells can be guided by this work as well.

ACKNOWLEDGMENTS

REFERENCES

[1]   Service, R. F., "Outlook Brightens for Plastic Solar Cells," Science, 332(6027), 293-293 (2011).
[2]   Lewis, N. S., "Toward cost-effective solar energy use," Science, 315(5813), 798-801 (2007).
[3]   Green, M. A., Emery, K., Hishikawa, Y., Warta, W., and Dunlop, E. D., "Solar cell efficiency tables (version 39)," Prog. Photovoltaics Res. Appl. , 20(1), 12-20 (2012).
[4]   Kroeze, J. E., Savenije, T. J., Vermeulen, M. J. W., and Warman, J. M., "Contactless determination of the photoconductivity action spectrum, exciton diffusion length, and charge separation efficiency in polythiophene-sensitized TiO2 bilayers," J. Phys. Chem. B 107(31), 7696-7705 (2003).
[5]   Haugeneder, A., Neges, M., Kallinger, C., Spirkl, W., Lemmer, U., Feldmann, J., Scherf, U., Harth, E., Gugel, A., and Mullen, K., "Exciton diffusion and dissociation in conjugated polymer fullerene blends and heterostructures," Phys. Rev. B, 59(23), 15346-15351 (1999).
[6]   Watkins, P. K., Walker, A. B., and Verschoor, G. L. B., "Dynamical Monte Carlo modelling of organic solar cells: The dependence of internal quantum efficiency on morphology," Nano Lett. , 5(9), 1814-1818 (2005).
[7]   Blom, P. W. M., deJong, M. J. M., and vanMunster, M. G., "Electric-field and temperature dependence of the hole mobility in poly(p-phenylene vinylene)," Phys. Rev. B, 55(2), R656-R659 (1997).
[8]   Li, G., Shrotriya, V., Yao, Y., and Yang, Y., "Investigation of annealing effects and film thickness dependence of polymer solar cells based on poly(3-hexylthiophene)," J. Appl. Phys. , 98(4), 043704 (2005).
[9]   Yang, Y., Mielczarek, K., Aryal, M., Zakhidov, A., and Hu, W., "Nanoimprinted Polymer Solar Cell," ACS Nano, 6(4), 2877-2892 (2012).
[10]   Chou, S. Y., Krauss, P. R., and Renstrom, P. J., "Imprint lithography with 25-nanometer resolution," Science, 272(5258), 85-87 (1996).
[11]   Guo, L. J., "Recent progress in nanoimprint technology and its applications," J. Phys. D: Appl. Phys. , 37(11), R123-R141 (2004).
[12]   Yang, Y., Aryal, M., Mielczarek, K., Hu, W., and Zakhidov, A., "Nanoimprinted P3HT/C60 solar cells optimized by oblique deposition of C60," J. Vac. Sci. Technol., B 28(6), C6M104-C6M107 (2010).
[13]   Aryal, M., Buyukserin, F., Mielczarek, K., Zhao, X., Gao, J., Zakhidov, A., and Hu, W., "Imprinted large-scale high density polymer nanopillars for organic solar cells," J. Vac. Sci. Technol., B 26(6), 2562-2566 (2008).

[14]   Zhou, M., Aryal, M., Mielczarek, K., Zakhidov, A., and Hu, W., "Hole mobility enhancement by chain alignment in nanoimprinted poly(3-hexylthiophene) nanogratings for organic electronics," J. Vac. Sci. Technol., B 28(6), C6M63-C6M67 (2010).

[15]   He, X., Gao, F., Tu, G., Hasko, D. G., Huettner, S., Greenham, N. C., Steiner, U., Friend, R. H., and Huck, W. T. S., "Formation of well-ordered heterojunctions in polymer: PCBM photovoltaic devices," Adv. Funct. Mater., 21(1), 139-146 (2011).

[16]   Wiedemann, W., Sims, L., Abdellah, A., Exner, A., Meier, R., Musselman, K. P., MacManus-Driscoll, J. L., Mueller-Buschbaum, P., Scarpa, G., Lugli, P., and Schmidt-Mende, L., "Nanostructured interfaces in polymer solar cells," Appl. Phys. Lett., 96(26), 263109 (2010).

[17]   Aryal, M., Trivedi, K., and Hu, W., "Nano-confinement induced chain alignment in ordered P3HT nanostructures defined by nanoimprint lithography," ACS Nano, 3(10), 3085-3090 (2009).

[18]   Hlaing, H., Lu, X., Hofmann, T., Yager, K. G., Black, C. T., and Ocko, B. M., "Nanoimprint-Induced Molecular Orientation in Semiconducting Polymer Nanostructures," ACS Nano, 5(9), 7532-7538 (2011).

[19]   Cui, D., Li, H., Park, H., and Cheng, X., "Improving organic thin-film transistor performance by nanoimprint-induced chain ordering," J. Vac. Sci. Technol., B 26(6), 2404-2409 (2008).

[20]   Zheng, Z., Yim, K.-H., Saifullah, M. S. M., Welland, M. E., Friend, R. H., Kim, J.-S., and Huck, W. T. S., "Uniaxial alignment of liquid-crystalline conjugated polymers by nanoconfinement," Nano Lett., 7(4), 987-992 (2007).

[21]   Hu, Z. J., Baralia, G., Bayot, V., Gohy, J. F., and Jonas, A. M., "Nanoscale control of polymer crystallization by nanoimprint lithography," Nano Lett., 5(9), 1738-1743 (2005).

[22]   Kline, R. J., McGehee, M. D., and Toney, M. F., "Highly oriented crystals at the buried interface in polythiophene thin-film transistors," Nat. Mater., 5(3), 222-228 (2006).

[23]   Chang, J.-F., Sun, B., Breiby, D. W., Nielsen, M. M., Sölling, T. I., Giles, M., McCulloch, I., and Sirringhaus, H., "Enhanced Mobility of Poly(3-hexylthiophene) Transistors by Spin-Coating from High-Boiling-Point Solvents," Chem. Mater., 16(23), 4772-4776 (2004).

[24]   Chen, D., Liu, F., Wang, C., Nakahara, A., and Russell, T. P., "Bulk Heterojunction Photovoltaic Active Layers via Bilayer Interdiffusion," Nano Lett., 11(5), 2071-2078 (2011).

[25]   Kim, D. H., Park, Y. D., Jang, Y., Yang, H., Kim, Y. H., Han, J. I., Moon, D. G., Park, S., Chang, T., Chang, C., Joo, M., Ryu, C. Y., and Cho, K., "Enhancement of Field-Effect Mobility Due to Surface-Mediated Molecular Ordering in Regioregular Polythiophene Thin Film Transistors," Adv. Funct. Mater., 15(1), 77-82 (2005).

[26]   Yang, Y., Lee, K., Mielczarek, K., Hu, W., and Zakhidov, A., "Nanoimprint of dehydrated PEDOT:PSS for organic photovoltaics," Nanotechnol., 22(48), 485301 (2011).

[27]   Sirringhaus, H., Brown, P. J., Friend, R. H., Nielsen, M. M., Bechgaard, K., Langeveld-Voss, B. M. W., Spiering, A. J. H., Janssen, R. A. J., Meijer, E. W., Herwig, P., and de Leeuw, D. M., "Two-dimensional charge transport in self-organized, high-mobility conjugated polymers," Nature, 401(6754), 685-688 (1999).

[28]   Chen, T. A., Wu, X. M., and Rieke, R. D., "Regiocontrolled Synthesis of Poly(3-alkylthiophenes) Mediated by Rieke Zinc - Their Characterization and Solid-state Properties," J. Am. Chem. Soc., 117(1), 233-244 (1995).

[29]   Zhokhavets, U., Erb, T., Hoppe, H., Gobsch, G., and Sariciftci, N. S., "Effect of annealing of poly(3-hexylthiophene)/fullerene bulk heterojunction composites on structural and optical properties," Thin Solid Films 496(2), 679-682 (2006).

[30]   Erb, T., Zhokhavets, U., Gobsch, G., Raleva, S., Stuhn, B., Schilinsky, P., Waldauf, C., and Brabec, C. J., "Correlation between structural and optical properties of composite polymer/fullerene films for organic solar cells," Adv. Funct. Mater., 15(7), 1193-1196 (2005).

[31]   Sirringhaus, H., Wilson, R. J., Friend, R. H., Inbasekaran, M., Wu, W., Woo, E. P., Grell, M., and Bradley, D. D. C., "Mobility enhancement in conjugated polymer field-effect transistors through chain alignment in a liquid-crystalline phase," Appl. Phys. Lett., 77(3), 406-408 (2000).

[32]   Li, G., Shrotriya, V., Huang, J. S., Yao, Y., Moriarty, T., Emery, K., and Yang, Y., "High-efficiency solution processable polymer photovoltaic cells by self-organization of polymer blends," Nat. Mater., 4(11), 864-868 (2005).

[33]   Prosa, T. J., Winokur, M. J., Moulton, J., Smith, P., and Heeger, A. J., "X-ray structural studies of poly(3-alkylthiophenes): an example of an inverse comb," Macromolecules, 25(17), 4364-4372 (1992).

[34]   Kim, Y., Choulis, S. A., Nelson, J., Bradley, D. D. C., Cook, S., and Durrant, J. R., "Device annealing effect in organic solar cells with blends of regioregular poly(3-hexylthiophene) and soluble fullerene," Appl. Phys. Lett., 86(6), 063502 (2005).

[35]   Brinkmann, M., and Wittmann, J. C., "Orientation of regioregular poly(3-hexylthiophene) by directional solidification: A simple method to reveal the semicrystalline structure of a conjugated polymer," Adv. Mater., 18(7), 860-863 (2006).

[36]   Coakley, K. M., Srinivasan, B. S., Ziebarth, J. M., Goh, C., Liu, Y. X., and McGehee, M. D., "Enhanced hole mobility in regioregular polythiophene infiltrated in straight nanopores," Adv. Funct. Mater., 15(12), 1927-1932 (2005).

[37]   Patterson, A. L., "The Scherrer Formula for X-Ray Particle Size Determination," Phys. Rev., 56(10), 978-982 (1939).

[38]   Ma, W. L., Yang, C. Y., Gong, X., Lee, K., and Heeger, A. J., "Thermally stable, efficient polymer solar cells with nanoscale control of the interpenetrating network morphology," Adv. Funct. Mater., 15(10), 1617-1622 (2005).

[39]   Shaheen, S. E., Brabec, C. J., Sariciftci, N. S., Padinger, F., Fromherz, T., and Hummelen, J. C., "2.5% efficient organic plastic solar cells," Appl. Phys. Lett., 78(6), 841-843 (2001).

[40]   Melzer, C., Koop, E. J., Mihailetchi, V. D., and Blom, P. W. M., "Hole transport in poly(phenylene vinylene)/methanofullerene bulk-heterojunction solar cells," Adv. Funct. Mater., 14(9), 865-870 (2004).

[41]   Alvin, M. G., and Albert, R., "Double Extraction of Uniformly Generated Electron - Hole Pairs from Insulators with Noninjecting Contacts," J. Appl. Phys., 42, 2823-2830 (1971).

Table 1. Summary of P3HT structures with different geometries.

Geometry (G) No.	1	2	3	4	5	6
width (*w*)/*spacing* (*p*) (nm)	-	280/280	210/210	60/80	60/80	60/80
height (*h*) (nm)	70 (thin film)	110	110	50	110	170
residual layer (*f*) (nm)	-	20	20	20	20	20
IEF (A/A_0)	1	1.39	1.52	1.71	2.57	3.43

Table 2. Summary of geometry effect on the sizes of crystallites formed by nanoimprint.

Geometry (G) No.	3	4	5	6
width/*spacing*/*height* (nm)	210/210/110	60/80/50	60/80/110	60/80/170
L_a (nm)	12.82	13.71	13.95	15.59
L_b (nm)	6.39	7.11	7.06	7.88

Table 3. Performance of P3HT/PCBM photovoltaic devices built on P3HT nanogratings with different geometries.

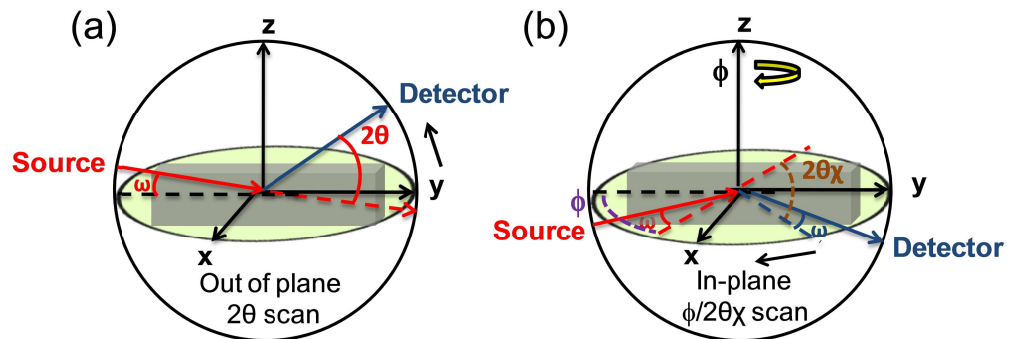| Device	D1	D2	D3	D4	D5	D6
width/*spacing*/*height* (nm)	70 nm thin film	280/280/110	210/210/110	60/80/50	60/80/110	60/80/170
IEF = A/A_0	1	1.39	1.52	1.71	2.57	3.43
V_{oc} (V)	0.53±0.01	0.54±0.01	0.53±0.01	0.56±0.01	0.55±0.01	0.57±0.00
J_{sc} (mA/cm^2)	5.47±0.67	6.42±0.06	6.48±0.09	7.42±0.42	8.23±0.19	9.16±0.30
FF	0.40±0.02	0.47±0.01	0.50±0.01	0.58±0.02	0.60±0.01	0.61±0.01
PCE (%)	1.16±0.14	1.61±0.02	1.72±0.05	2.40±0.10	2.67±0.08	3.16±0.07

Figure 1. Schematic of GIXRD setups for (a) out-of-plane measurement with scan axis of 2θ and (b) in-plane measurement with scan axis of φ/2θχ. The incident X-rays in both setups are at a small incident angle ω to the plane of sample surfaces.
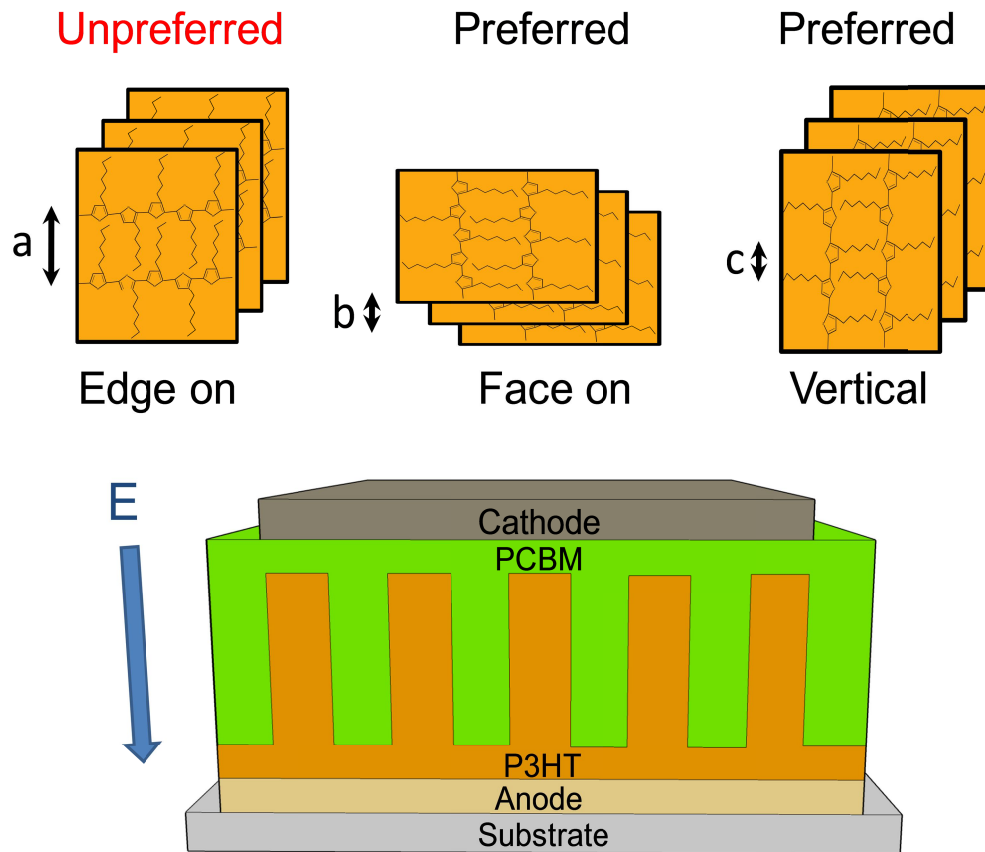
Figure 2. Schematic of edge-on, face-on and vertical chain orientations of P3HT molecules which are sandwiched vertically between cathode and anode. Face-on and vertical orientations are preferred for hole transport due to theirs short hopping distances b and c, respectively, along the vertical direction of electric field E, compared to the un-preferred edge-on with a large hopping distance a.
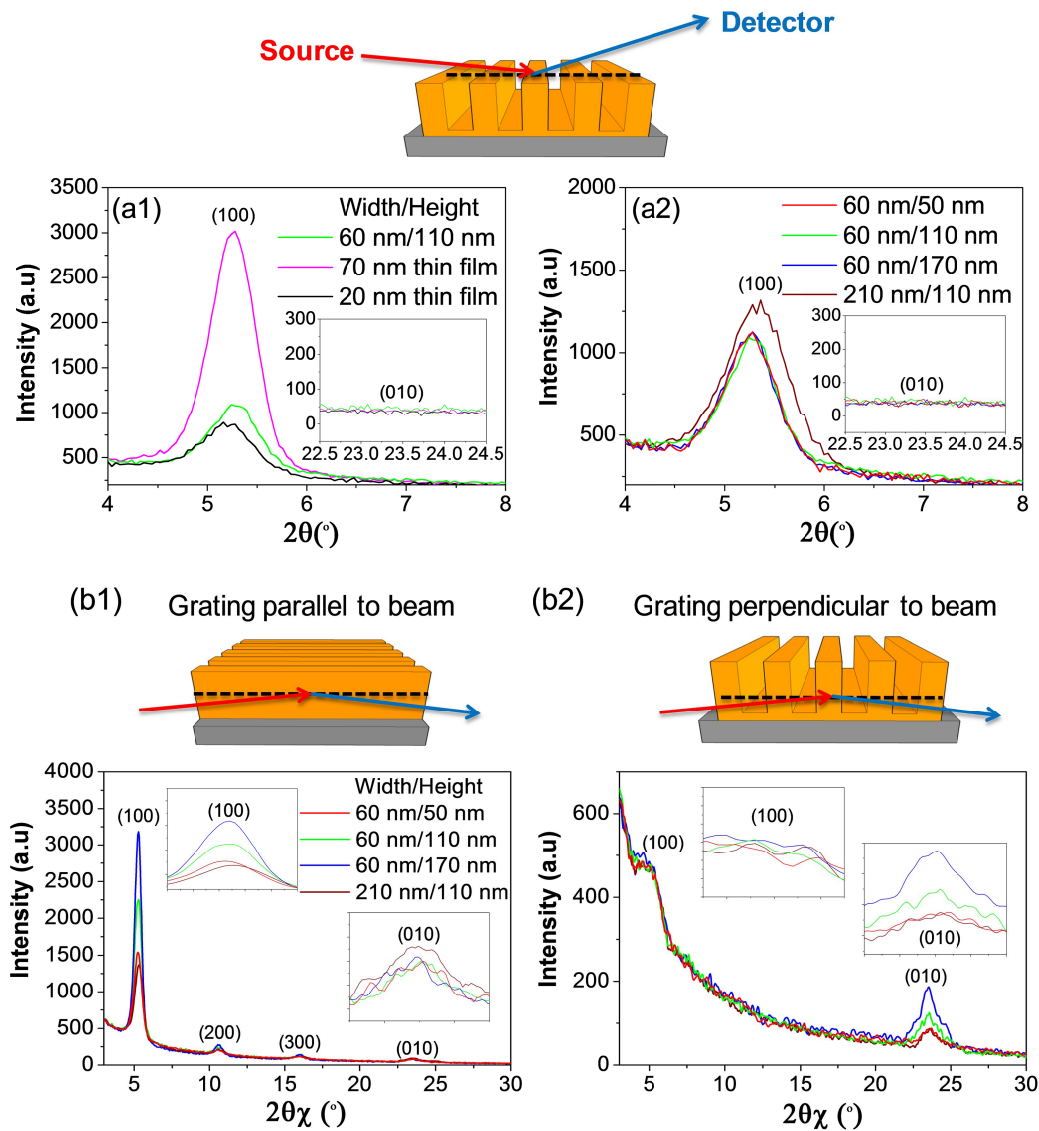
Figure 3. (a) Out-of-plane GIXRD measurement of P3HT chain orientations within: (a1) nanogratings and non-imprinted thin films which are as thick as the nanostructures before imprint and their *residual layer*, respectively; (a2) nanogratings with different *heights* and *widths*. (b) In-plane GIXRD measurement of P3HT chain orientations with imprinted gratings (b1) parallel and (b2) perpendicular to the incident X-ray beam. The side figures in (a1) and (a2) show the views of the (010) peaks and in (b1) and (b2) show the magnified views of the (100) peaks and (010) peaks, respectively.

(a)

(b)
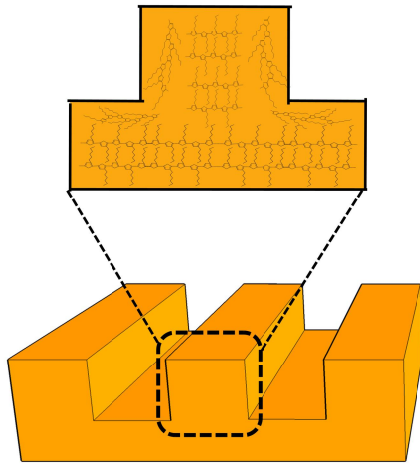
Partially aligned vertical orientation
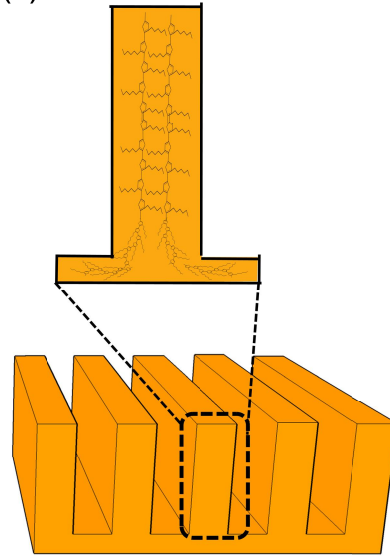
Fully aligned vertical orientation

Figure 4. Schematic of imprinted P3HT nanostructures with different geometries and their effects on chain alignment/orientations: (a) the partially aligned vertical orientations which only exist in regions close to the mold trenches while edge-on orientations remain in the middle within wide and low nanostructures and (b) full aligned vertical orientations within the high and narrow nanostructures.
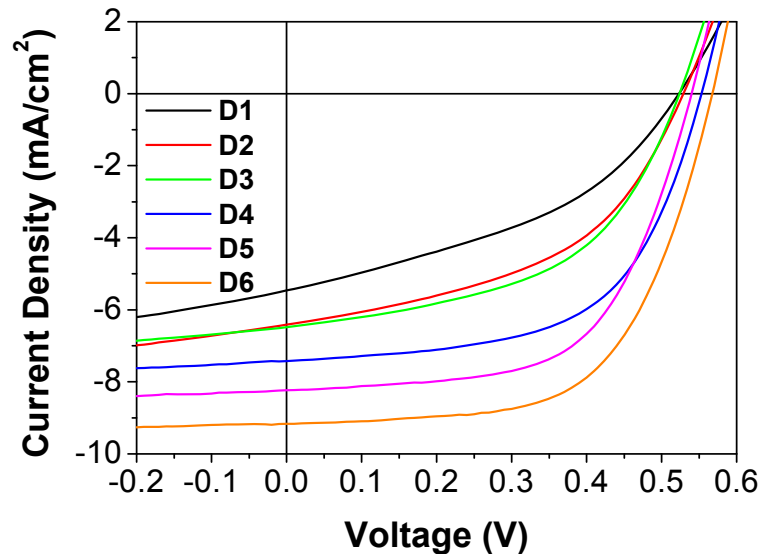
Figure 5. *J-V* characteristics of P3HT/PCBM solar cells built with different P3HT geometries: non-imprinted 70 thin film (D1), nanogratings with *width*/*spacing* and *height* of 280 nm and 110 nm (D2), 210 nm and 110 nm (D3), 60 nm and 50 nm (D4), 60 nm and 110 nm (D5) and 60 nm and 170 nm (D6), respectively.